$\Delta(E + ZPE) \, \text{kcal} \cdot \text{mol}^{-1}$

without
H_2O
$(H_2O)_2$
H_2SO_4

0.0

$N_2O_4 + NH_3 + X$

3.2

−0.4

−0.4

−4.6

−9.4

−9.2

−14.9

−15.4

$HNO_3 + NH_2NO$

$HNO_3 \cdots H_2O + NH_2NO$

$HNO_3 \cdots (H_2O)_2 + NH_2NO$

$HNO_3 \cdots H_2SO_4 + NH_2NO$

$N_2O_4 + NH_3$

NO_2 dimer

catalysts

$HNO_3 + NH_2NO$

acid rain

Showcasing research from Professor Tianlei Zhang's laboratory, School of Chemistry & Environment Science, Shaanxi University of Technology, Hanzhong, China.

A possible atmospheric source of HNO_3: the ammonolysis reaction of t-N_2O_4 in the presence of water monomer, water dimer, and sulfuric acid

The effect of H_2O, $(H_2O)_2$ and H_2SO_4 on the ammonolysis of t-N_2O_4 to form HNO_3 was studied by a quantum chemical method and Master equation rate calculations. Results reveal that the ammonolysis of t-N_2O_4 with $(H_2O)_2$ and H_2SO_4 are barrierless or nearly barrierless reactions. Considering the effective rate constant, $(H_2O)_2$ outperforms the other catalysts in the range of 280-320 K (0 km). Moreover, the effect of H_2SO_4 is obvious at higher altitudes of 5-30 km. In general, this work will give new insights into how the neutral and acidic catalysts affect the formation of HNO_3.

ROYAL SOCIETY OF CHEMISTRY

rsc.li/esatmospheres

Check for updates

A possible atmospheric source of HNO₃: the ammonolysis reaction of *t*-N₂O₄ in the presence of water monomer, water dimer, and sulfuric acid†

Ruxue Mu,‡[a] Weixin Zhou,‡[a] Zhaozhao Hong,[a] Rui Wang, [ID][a] Quan Liu, [ID][a] Qiang Zhang, [ID][a] Min Jiang,[a] Balaganesh Muthiah [ID][b] and Tianlei Zhang [ID]*[a]

Although the ammonolysis of *t*-N₂O₄ is one of the potential sources of HNO₃ formation, the available studies have only focused on its naked reaction. Herein, the effect of important neutral and acidic trace gases, water monomer, water dimer, and sulfuric acid, on the formation of HNO₃ from the ammonolysis of *t*-N₂O₄ was studied by the quantum chemical method of CCSD(T)/aug-cc-pVTZ//B3LYP-D3/6-311++G(3df,2pd) and the Master equation/Rice–Ramsperger–Kassel–Marcus (ME/RRKM) rate calculations. The quantum chemical results revealed that the ammonolysis of *t*-N₂O₄ with $(H_2O)_2$ and H_2SO_4 are barrierless or nearly barrierless reactions, potentially lowering the energy barrier to 3.4–4.1 kcal mol⁻¹. The calculated effective rate constant illustrates that $(H_2O)_2$ (100% RH) dominates over H_2O and H_2SO_4 within the range of 280–320 K (0 km), with an effective rate constant that is 1–3 orders of larger magnitude, whereas H_2SO_4 (10⁸ mol cm⁻³) is the most favorable catalyst within the troposphere between 5 and 30 km. However, the contributions of H_2O, $(H_2O)_2$, and H_2SO_4 are not apparent in the gas-phase ammonolysis of *t*-N₂O₄ within the range of 213–320 K and 0–30 km because their effective rate constants were at least 4 orders of magnitude lower than the corresponding rate constant of the ammonolysis of *t*-N₂O₄. In general, the current findings shed fresh light on neutral (H_2O and $(H_2O)_2$) and acidic (H_2SO_4) catalysts that not only affect energy barriers but also have an impact on the ammonolysis of *t*-N₂O₄ in neutral and acidic conditions.

Environmental significance

Nitrogen tetroxide (N_2O_4) is considered to be a dimer of nitrogen dioxide (NO_2) and plays an important role in the formation of acid rain. The fact is that the ammonolysis of *t*-N₂O₄ is one of the potential sources of HNO₃ formation; thus, the effort of water monomer, water dimer, and sulfuric acid on the ammonolysis of *t*-N₂O₄ was studied by quantum chemical method and Master equation rate calculations. The quantum chemical results reveal that the ammonolysis of *t*-N₂O₄ with $(H_2O)_2$ and H_2SO_4 are barrierless or nearly barrierless reactions. In terms of the effective rate constant, $(H_2O)_2$ outperforms the other catalysts in the temperature range 280–320 K (0 km). Moreover, the effect of H_2SO_4 on the ammonolysis reaction of *t*-N₂O₄ is obvious at higher altitudes of 5–30 km. In general, this work will give a new insights into how the neutral and acidic catalysts affect the formation of HNO₃.

1. Introduction

Nitrogen dioxide (NO_2),[1] as one of the most significant NO_x, is not only a precursor to the photochemical formation of ozone in the troposphere,[2] but it can also contribute to the formation of photochemical smog and cause significant health and

[a]*Institute of Theoretical and Computational Chemistry, Shaanxi Key Laboratory of Catalysis, School of Chemical & Environment Science, Shaanxi University of Technology, Hanzhong, Shaanxi 723000, P. R. China. E-mail: ztianlei88@l63.com; Fax: +86-916-2641083; Tel: +86-916-2641083*

[b]*Department of Chemical Engineering, National Taiwan University, Taipei 106, Taiwan*

† Electronic supplementary information (ESI) available. See DOI: https://doi.org/10.1039/d3ea00095h

‡ Ruxue Mu and Weixin Zhou have contributed equally to this work.

environmental hazards.[3] Nitrogen tetroxide (N_2O_4), a dimer of nitrogen dioxide (NO_2),[4] can be used for nitration, nitrosation, and oxidation.[5] In addition, N_2O_4 is an oxidizing agent for auto-igniting fuels and plays an important role in the formation of acid rain.[6] Due to the fact that N_2O_4 is a highly toxic chemical species that hinders experimental studies,[7] quantum calculations are a trend in current research to probe the N_2O_4-related reaction mechanisms. As the most major loss route of N_2O_4 in the atmosphere, the hydrolysis of N_2O_4 is potentially important in the lower atmosphere and plays an important role in the formation of HONO, a major source of OH pollution in the urban atmosphere.[8,9]

Several investigations have shown that the less stable *t*-N₂O₄ (*trans*-N₂O₄) is substantially more reactive than *s*-ONONO₂ (symmetric N₂O₄); hence, it was selected as a starting point for

© 2023 The Author(s). Published by the Royal Society of Chemistry

Environ. Sci.: Atmos., 2023, 3, 1407–1417 | 1407

studying the hydrolysis of NO$_2$ dimers.[9–12] The reaction barrier for the hydrolysis of t-N$_2$O$_4$ to form HONO was in the range of 10.8–11.9 kcal mol^{-1} at different theoretical levels.[9,11,12] Several groups reported that using H$_2$O and (H$_2$O)$_2$ as catalysts stabilized the reactant complexes by 3.5–6.9 kcal mol^{-1} and reduced the energy barrier to 6.2 kcal mol^{-1}. Consequently, Zhang et $al.$[9] revealed that, for the hydrolysis of t-N$_2$O$_4$, the H$_2$SO$_4$ catalyst is more effective than H$_2$O and (H$_2$O)$_2$ catalysts, resulting in not only a higher binding energy of 15.0 kcal mol^{-1} for the reactant complex but also a lower energy barrier of 3.8 kcal mol^{-1}.

In the atmosphere, the hydrolysis of t-N$_2$O$_4$ to produce HONO is the most major loss route of t-N$_2$O$_4$.[10,11] As a complement to the loss of t-N$_2$O$_4$, the ammonolysis reaction of t-N$_2$O$_4$ can form HNO$_3$,[13] which could be competitive with the main source of HNO$_3$, the gas-phase reaction of NO$_2$ with the hydroxyl (OH) radical[8,14] during the day and the hydrolysis reaction of N$_2$O$_5$[15–17] at night, in polluted areas of NH$_3$. The ammonolysis of t-N$_2$O$_4$ (shown in eqn (1) and (2)) investigated by Lin et $al.$[13] reveals that the energy barrier of the t-N$_2$O$_4$ + NH$_3$ reaction was determined to be 5.3 kcal mol^{-1} and the corresponding rate constant at low temperature was not pressure-dependent. As far as we know, the effect of neutral and acidic gases on the ammonolysis of t-N$_2$O$_4$, which plays a significant catalytic role in hydrogen abstraction reactions,[9,15,18–37] has not been explored.

$$NO_2 + NO_2 \leftrightarrow t\text{-}N_2O_4 \tag{1}$$

$$t\text{-}N_2O_4 + NH_3 \rightarrow HNO_3 + NH_2NO \tag{2}$$
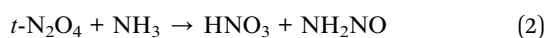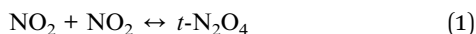
As in the previous studies on N$_2$O$_4$ + H$_2$O,[11,12] HO$_2$ + NO$_2$,[38] H$_2$CO + NH$_3$,[39] and SO$_2$ + NO$_2$[40] reactions, water molecules were found to play an essential role in enhancing the stability of pre-reactive complexes and lowering the apparent activation energies of the transition states. In addition to water monomer, some recent works addressed the potential role of water dimer,[18,41] which may play a significant catalytic role in hydrogen abstraction reactions because its concentrations can reach 9 × 10^{14} mol cm^{-3}.[42,43] Aside from water monomer and water dimer, acidic[9,15,30–37] gas species in the atmosphere may also be effective in lowering the energy barriers for hydrogen transfer reactions[30–34] and atmospheric hydrolysis reactions[9,15,35–37] in the gas phase. The presence of H$_2$SO$_4$[37,44] in the atmosphere was considered to be a more effective catalyst than neutral catalysts,[25,28–30,33,45] which not only greatly reduces the energy barriers[27,28,33] but also facilitates the transfer of hydrogen,[30–33,46] and thus, H$_2$SO$_4$ was regarded as either good acceptors or good donors of H in the catalytic gas reactions. These situations stimulated our interest in studying the ammonolysis of t-N$_2$O$_4$ by neutral (H$_2$O and (H$_2$O)$_2$) and acidic (H$_2$SO$_4$) gases.

In this work, using global minimum searching combined with quantum chemical methods, we first obtained the stable structures of the reactant complexes of t-N$_2$O$_4$···NH$_3$···X (X = H$_2$O, (H$_2$O)$_2$, and H$_2$SO$_4$). The ammonolysis of t-N$_2$O$_4$ in the presence of X was then studied using the stable molecular clusters t-N$_2$O$_4$···NH$_3$···X. Finally, the effective rate constant for

the ammonolysis of t-N$_2$O$_4$ with X was estimated at temperatures ranging from 213 to 320 K and altitudes ranging from 0 to 30 km.

2. Calculation details

2.1 Electronic structure calculations

The molecular geometries of the isolated reactants, pre-reactive complexes, transition states, post-reactive complexes, and products of the ammonolysis reaction of t-N$_2$O$_4$ without and with X were optimized using the B3LYP-D3 method[47–53] with 6-311++G(3df,2pd) basis set in Gaussian 09 suites.[54] The D3 method has been reliably utilized to describe the noncovalent interaction and the equilibrium structure of atmospheric clusters and reactions.[51,55] Notably, the keyword "stable = opt" is added in the calculations at the B3LYP-D3/6-311++G(3df,2pd) level to ensure that all the geometries are stable. Frequency calculations were calculated at the same level for all stationary points to check that all transition states have the same character as a first-order saddle point with a single imaginary frequency and that other stationary points correspond to minima on potential energy surfaces (PESs). The scaling factor employed to adjust the ZPEs was 0.969.[56,57] To ensure that the optimized transition state connects the desired pre- and post-reactive complexes, intrinsic reaction coordinate (IRC) calculations[58–60] were performed at the same level. To improve the accuracy of the relative energies, single-point energy calculation was performed at the CCSD(T)/aug-cc-pVTZ[61–63] level by using the Gaussian 09 software.[54] It was noted that the T_1 diagnostic values for closed-shell in Table S3† were 0.02 less than the standard value,[64,65] showing the multireference calculations for recovering non-dynamical correlation were not a problem, and the single reference method of CCSD(T)/aug-cc-pVTZ is reliable to single point energy calculation.

Global minimum searching combined with quantum chemical methods was employed to obtain the most stable structures of the reactant complexes of t-N$_2$O$_4$···NH$_3$···X. Initially, 500 structures with low energies were auto-produced by ABCluster software[66,67] with TIP4P[68,69] model for H$_2$O, (H$_2$O)$_2$, and CHARMM[70] force field for t-N$_2$O$_4$, NH$_3$, and H$_2$SO$_4$. Then, pre-optimized by the semi-empirical method of PM7[71] in MOPAC 2016.[72] Next, the structures with the N(t-N$_2$O$_4$)···N(NH$_3$) interaction of electron donor–acceptor (EDA) and facilitating the transfer of hydrogen atom from t-N$_2$O$_4$ to NH$_3$ were selected to optimize at the B3LYP-D3/6-311+G(d,p) level. Subsequently, 50 isomers with an order of electronic energies were chosen to optimize at the level of B3LYP-D3/6-311+G(2d,2p). Finally, the global minimum isomers within 5.0 kcal mol^{-1} (the electric energy) were re-optimized at the B3LYP-D3/6-311++G(3df,2pd) level.

2.2 Rate constant calculations

The rate constants for the ammonolysis reaction of t-N$_2$O$_4$ without and with X were calculated in two steps. First, the high-pressure-limit (HPL) rate constants were calculated by using the VRC-VTST calculations in Polyrate 2017 software.[73] The details

of VRC-VTST can be seen in Table S7 of the ESI.† Then, based on the HPL rate constants, the rate constants for the ammonolysis reaction of t-N_2O_4 without and with X at different temperatures and pressures were calculated using the Master Equation Solver for Multi-Energy Well Reactions (MESMER) program.[74] The Inverse Laplace Transform (ILT) approach was used to analyze the barrierless step from distinct reactants to the pre-reactive complex.[75,76] Meanwhile, the transition step from the pre-reactive complex to the post-reactive complex occurring through the transition state was applied to the RRKM theory.[77,78] ILT methods and RRKM theory can be, respectively, expressed in eqn (3) and (4).

$$k(E) = \frac{W(E - E_0)}{h\rho(E)} \tag{3}$$

$$k^\infty(\beta) = \frac{1}{Q(\beta)} \int_0^\infty k(E)\rho(E)\exp(-\beta E)\,dE \tag{4}$$

In eqn (3) and (4), where $W(E - E_0)$ is the rovibrational sum of states (SOS) at the optimized transition state (TS) geometry, E_0 is the reaction threshold energy, h is Planck's constant, $\rho(E)$ is the density of rovibrational states of the reactant, and $Q(\beta)$ is the corresponding canonical partition function. Moreover, the electronic geometries, vibrational frequencies, and rotational constants were calculated at the B3LYP-D3/6-311++G(3df,2pd) level, and single-point energy calculations were refined at the CCSD(T)/aug-cc-pVTZ level for the modeling. The one-dimensional asymmetric Eckart potential was used to treat the tunneling effect in the RRKM calculation. In addition, the Lennard-Jones (L-J) parameters $\varepsilon/k_B = 71.4$ K and $\sigma = 3.798$ Å were used for N_2,[79] $\varepsilon/k_B = 200.0$ K and $\sigma = 3.50$ Å were used for t-N_2O_4,[80] while $\varepsilon/k_B = 481.0$ K and $\sigma = 2.92$ Å were estimated for NH_3.[80]

3. Results and discussions

The pre-reactive complex in each reaction channel was denoted by "IM" followed by a number, whereas the transition state and post-reactive complexes were denoted by "TS" and "IMF", respectively. Species in the presence of H_2O, $(H_2O)_2$, and H_2SO_4 were denoted by the suffixes "WM", "WD", and "SA".

3.1 Mechanism and rate constants for the ammonolysis reaction of t-N_2O_4

The ammonolysis reaction of t-N_2O_4 has been extensively investigated from the theoretical viewpoint.[13] Here, this reaction has been reinvestigated at the CCSD(T)/aug-cc-pVTZ//B3LYP-D3/6-311++G(3df,2pd) level to check the catalytic effect of X. Our results shown in Fig. 1 were found to be very mechanistically and energetically similar to the work reported by Lin $et\ al.$[13] All the relative energy values qualitatively matched (see Table S2†). As seen in Fig. 1, the t-N_2O_4 + NH_3 reaction occurred through a ring formation mechanism, resulting in the formation of a six-membered ring complex t-$N_2O_4 \cdots NH_3$ with a binding energy of 0.5 kcal mol^{-1}. Then, the terminal O1 atom of t-N_2O_4 abstracts the H atom of NH_3 along with the N–N bond formation to form the product complex $HNO_3 \cdots NH_2NO$. From an energy point of view, the barrier height of the t-N_2O_4 + NH_3 reaction was 3.7 kcal mol^{-1}, revealing that t-N_2O_4 can easily react with NH_3 in the gas phase.

The calculated rate constants for the ammonolysis reaction of t-N_2O_4 are listed in Table 1. In the ammonolysis reaction of t-N_2O_4, the hindered internal rotation (HIR)[77,81–86] correction at 760 Torr has a moderate effect, increasing the rate constants by a factor of 1.25 to 1.28. Meanwhile, the almost unchanged rate constants for the ammonolysis reaction of t-N_2O_4 at different atmospheric pressures revealed that the pressure (10–760 Torr)[87] has little effect on the ammonolysis reaction of t-N_2O_4 within the temperature range of 280–320 K.[88,89]

3.2 Mechanism and rate constants for the ammonolysis reaction of t-N_2O_4 with H_2O and $(H_2O)_2$

Fig. 2a and b show the ammonolysis reaction of t-N_2O_4 assisted by H_2O (Channel WM) and $(H_2O)_2$ (Channel WD), where both H_2O and $(H_2O)_2$ served as a "bridge" to promote hydrogen atom transfer from the N3 atom of NH_3 to the terminal O1 atom of t-N_2O_4. In the case of Channel WM, the reaction can occur either (a) between NH_3 and monohydrated t-N_2O_4 (t-$N_2O_4 \cdots H_2O$) or (b) between hydrated NH_3 ($NH_3 \cdots H_2O$) and t-N_2O_4. The binding energy of t-$N_2O_4 \cdots H_2O$ was 2.9 kcal mol^{-1}, which was consistent with the previously calculated value of 3.5 kcal mol^{-1} at the CCSD(T)-F12a/cc-pVDZ-F12//M06-2X/6-311++G(3df,2pd) level.[9]

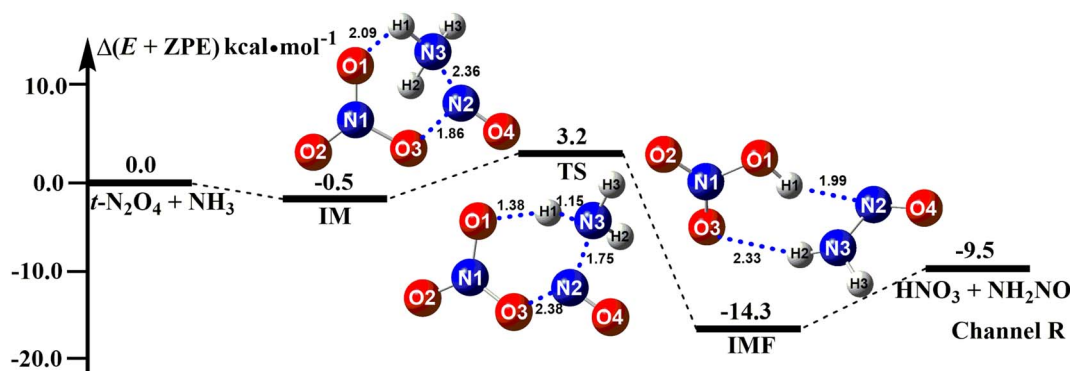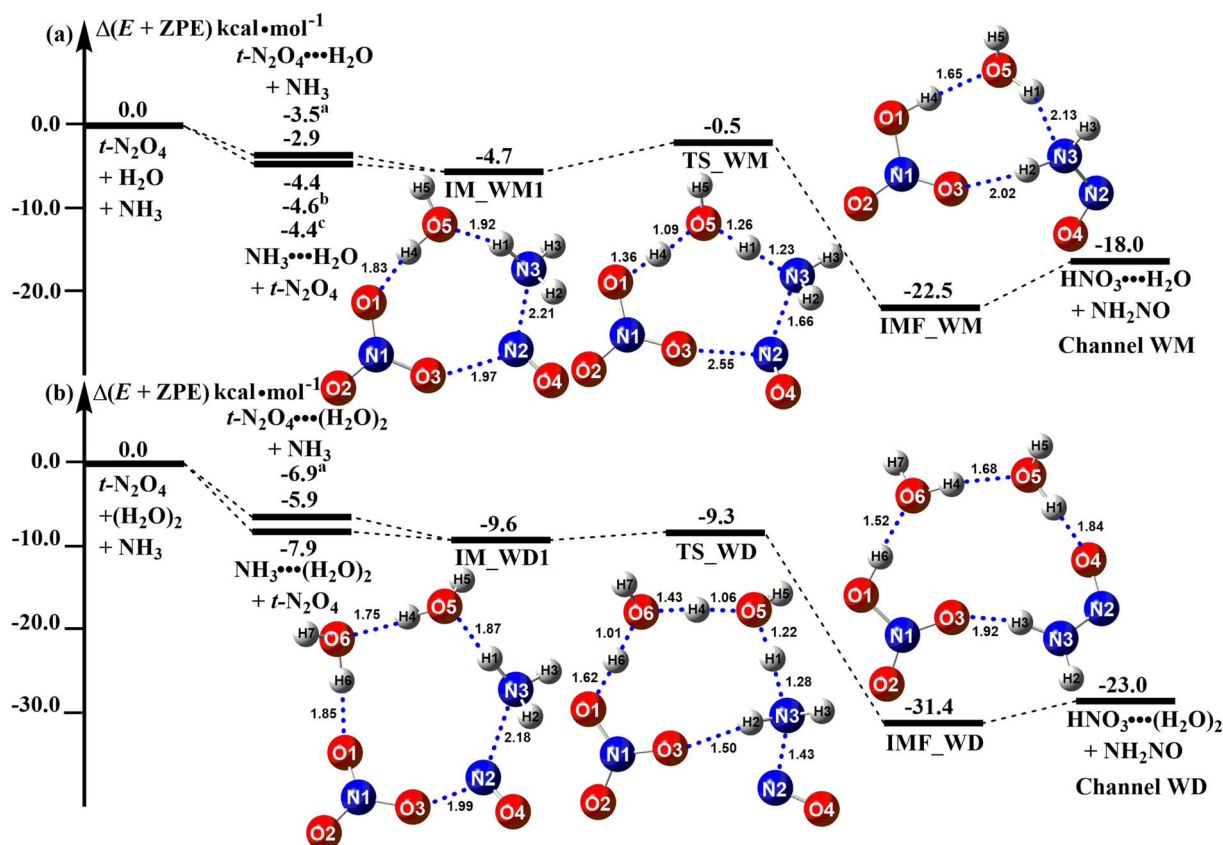Fig. 1 Potential energy profiles for the t-N_2O_4 + $NH_3 \rightarrow HNO_3 + NH_2NO$ reaction at the CCSD(T)/aug-cc-pVTZ//B3LYP-D3/6-311++G(3df,2pd) level.

Table 1 The rate constants (k_R) (cm^3 mol^{-1} s^{-1}) for the t-N$_2$O$_4$ + NH$_3$ reaction without and with HIR treatments within the temperature range of 280–320 K and pressure range of 10–760 Torr

	HIR impact[a]			Pressure impact				
T (K)	With HIR treatments	Without HIR treatments	Factor[b]	10 Torr	50 Torr	100 Torr	300 Torr	760 Torr
280	6.67×10^{-17}	5.20×10^{-17}	1.28	5.03×10^{-17}	5.14×10^{-17}	5.16×10^{-17}	5.18×10^{-17}	5.20×10^{-17}
290	7.81×10^{-17}	6.13×10^{-17}	1.27	5.90×10^{-17}	6.07×10^{-17}	6.10×10^{-17}	6.12×10^{-17}	6.13×10^{-17}
298	8.80×10^{-17}	6.95×10^{-17}	1.27	6.65×10^{-17}	6.88×10^{-17}	6.92×10^{-17}	6.94×10^{-17}	6.95×10^{-17}
300	9.06×10^{-17}	7.17×10^{-17}	1.26	6.84×10^{-17}	7.09×10^{-17}	7.13×10^{-17}	7.16×10^{-17}	7.17×10^{-17}
310	1.04×10^{-16}	8.32×10^{-17}	1.26	7.84×10^{-17}	8.20×10^{-17}	8.26×10^{-17}	8.30×10^{-17}	8.32×10^{-17}
320	1.19×10^{-16}	9.57×10^{-17}	1.25	9.40×10^{-17}	9.40×10^{-17}	9.55×10^{-17}	9.55×10^{-17}	9.57×10^{-17}

[a] HIR impact represents the hindered internal rotations treatment. [b] Factor denotes the rate ratio between with HIR treatments and without HIR treatments.

Fig. 2 Potential energy profiles for the t-N$_2$O$_4$ + NH$_3$ → HNO$_3$ + NH$_2$NO reaction catalyzed by H$_2$O and (H$_2$O)$_2$ at the CCSD(T)/aug-cc-pVTZ//B3LYP-D3/6-311++G(3df,2pd) level (a–c) denotes the values respectively reported from ref. 9, 90, and 91.

The binding energy of NH$_3$···H$_2$O was 4.4 kcal mol^{-1}, which agreed well with the calculated values of 4.4–4.6 kcal mol^{-1}.[90,91] The stability of NH$_3$···H$_2$O was 1.5 kcal mol^{-1} higher than that of t-N$_2$O$_4$···H$_2$O. So, the ammonolysis of t-N$_2$O$_4$ in the presence of H$_2$O mainly takes place *via* the collision of NH$_3$···H$_2$O with t-N$_2$O$_4$ to form the quasi-planar eight-membered ring reactant complex IM_WM1. The energy of the reactant complex IM_WM1 was 4.7 kcal mol^{-1} lower than that of the isolated reactants t-N$_2$O$_4$ + H$_2$O + NH$_3$. In the complex IM_WM1, H$_2$O played the roles of a single acceptor and donor of hydrogen

bonds. After the formation of the complex IM_WM1, the reaction proceeded to form a hydrogen-bonded complex, HNO$_3$···H$_2$O···NH$_2$NO (denoted IMF_WM), through the transition state TS_WM, with an energy barrier of 4.2 kcal mol^{-1}.

The reaction t-N$_2$O$_4$ + NH$_3$ + (H$_2$O)$_2$ can be initiated by the reactant complex IM_WD1, which can be formed from t-N$_2$O$_4$···(H$_2$O)$_2$ + NH$_3$ or t-N$_2$O$_4$ + NH$_3$···(H$_2$O)$_2$. It is clear from Fig. 2b that NH$_3$ was most likely bound to (H$_2$O)$_2$ prior to t-N$_2$O$_4$. The reactant complex IM_WD1 has a quasi-planar structure similar to that of complex IM_WM1 and can be regarded as H$_2$O in

1410 | *Environ. Sci.: Atmos.*, 2023, **3**, 1407–1417

© 2023 The Author(s). Published by the Royal Society of Chemistry

IM_WM1, which was replaced by $(H_2O)_2$. The binding energy of IM_WD1 was 1.7 kcal mol^{-1} from t-N_2O_4 + NH_3···$(H_2O)_2$. After complex IM_WD1, the ammonolysis reaction of t-N_2O_4 with $(H_2O)_2$ can form the product complex HNO_3···$(H_2O)_2$···NH_2NO (labeled as IMF_WD) through the transition state TS_WD with an energy barrier of 0.3 kcal mol^{-1}. Three hydrogen atom transfer mechanisms occurred at TS_WD, as well as the simultaneous formation of the N(2)···N(3) bond. In comparison to H_2O in Channel WM, $(H_2O)_2$ in Channel WD played a more obvious catalytic role in promoting the ammonolysis reaction of t-N_2O_4. When $(H_2O)_2$ was used as a catalyst in Channel WD, it stabilized the reactant complex by a further 4.9 kcal mol^{-1} and decreased the reaction barrier by 3.9 kcal mol^{-1}. The more pronounced catalytic effect of $(H_2O)_2$ could be attributed to two factors. On the one hand, $(H_2O)_2$ may improve the N(t-N_2O_4)···N(NH_3) interaction compared to H_2O. For example, in the reactant complex IM_WD1, the strengthening of the N(t-N_2O_4)···N(NH_3) interaction was shown by the shortening of the bond distance N(2)···N(3) (2.18 Å, shown in Fig. 2b), which is less than the corresponding value in the reactant complex IM_WM1 (2.21 Å, shown in Fig. 2a). On the other hand, when H_2O was replaced by $(H_2O)_2$, however, the transition state extended from an eight-member ring (TS_WM) to a ten-member ring (TS_WD). This structural change reduces the ring tension of the transition state to a certain extent, lowering the reaction energy barrier.

As shown in Table 2, within the range of 213–320 K and 0–30 km,[88,89] the rate constant for the ammonolysis reaction of t-N_2O_4 assisted by H_2O (k_{WM}) was predicted to be 3.94×10^{-20} to 1.93×10^{-19} cm^3 mol^{-1} s^{-1}, which was 2–3 orders of magnitude lower than that of the naked ammonolysis reaction of t-N_2O_4. The calculated rate constant for the ammonolysis reaction of t-N_2O_4 assisted by $(H_2O)_2$ (k_{WD}) was 3.66×10^{-16} to 1.98×10^{-15} cm^3 mol^{-1} s^{-1}, which was 1–2 orders of magnitude greater than the naked ammonolysis reaction of t-N_2O_4. The ammonolysis reaction of t-N_2O_4 assisted by $(H_2O)_2$ was more kinetically favorable than the ammonolysis reaction of t-N_2O_4 with H_2O, with a rate constant that was 3–5 orders of magnitude greater.

3.3 Mechanism and rate constants for the ammonolysis reaction of t-N_2O_4 with H_2SO_4

As shown in Fig. S3,† nine geometrical isomers of the reactant complex t-N_2O_4···NH_3···H_2SO_4 (labeled as IM_SAn, $n = 1$–9) were found at the B3LYP-D3/6-311++G(3df,2pd) level, with complex IM_SA1 being the most stable. Based on complex IM_SA1, Fig. 3 presents the potential energy surface (PES) for the ammonolysis of t-N_2O_4 in the presence of H_2SO_4 (Channel SA). In the case of Channel SA, the reaction can occur (a) between NH_3 and t-N_2O_4···H_2SO_4 or (b) between t-N_2O_4 and NH_3···H_2SO_4. The binding energy of NH_3···H_2SO_4 was 14.7 kcal mol^{-1}, which was in good agreement with the previously reported value.[92] The large binding energy of NH_3···H_2SO_4 indicates that in the reaction of t-N_2O_4 + NH_3 + H_2SO_4, NH_3 is easily bound to the isolated H_2SO_4. In this sense, the ammonolysis reaction of t-N_2O_4 with H_2SO_4 mainly takes place via the collision of t-N_2O_4 with NH_3···H_2SO_4, resulting in the reactant complex IM_SA1.

The energy of the reactant complex IM_SA1 was 15.0 kcal mol^{-1} lower than that of the separate reactants t-N_2O_4, NH_3, and H_2SO_4. In the complex IM_SA1, H_2SO_4 served as a single donor and acceptor of hydrogen bonds to form a ring-like structure with the binary complex of t-N_2O_4···NH_3. The stability of complex IM_SA1 increased by 5.4–10.3 kcal mol^{-1} when compared to the reactant complexes IM_WM1 and IM_WD1, with the distance of the N(t-N_2O_4)···N(NH_3) bond reduced by 0.01–0.04 Å. After the formation of the complex IM_SA1, Channel SA proceeded through the transition state TS_SA to form a ten-membered ring hydrogen-bonded complex HNO_3···H_2SO_4···NH_2NO (labeled as IMF_SA). Similar to the transition state TS_WM described above, TS_SA was in the middle of a double hydrogen atom transfer process, with the H_2SO_4 moiety serving as a bridge for the hydrogen transfer. From the viewpoint of the energy barrier height, Channel SA was a barrierless process. In comparison to H_2O and $(H_2O)_2$, H_2SO_4 could lower the energy barrier, at least by 0.7–4.6 kcal mol^{-1}. Complex IMF_SA showed a ten-membered ring structure. It had a binding energy of 28.0 kcal mol^{-1} to the separate reactants t-N_2O_4, NH_3, and H_2SO_4, which was 13.0 kcal mol^{-1} lower than the

Table 2 Calculated rate constants (k, cm^3 mol^{-1} s^{-1}) for the t-N_2O_4 + NH_3 reaction with H_2O, $(H_2O)_2$, and H_2SO_4 calculated by master equation within the range of 213–320 K and 0–30 km[a,b]

Altitude	T (K)	k_R	k_{WM}	k_{WD}	k_{SA}
0 km	280	5.20×10^{-17}	1.16×10^{-19}	6.05×10^{-16}	1.49×10^{-16}
	290	6.13×10^{-17}	1.33×10^{-19}	5.29×10^{-16}	1.50×10^{-16}
	298	6.95×10^{-17}	1.48×10^{-19}	4.76×10^{-16}	1.50×10^{-16}
	300	7.17×10^{-17}	1.52×10^{-19}	4.64×10^{-16}	1.51×10^{-16}
	310	8.32×10^{-17}	1.72×10^{-19}	4.11×10^{-16}	1.52×10^{-16}
	320	9.57×10^{-17}	1.93×10^{-19}	3.66×10^{-16}	1.54×10^{-16}
5 km	259.3	3.59×10^{-17}	8.59×10^{-20}	8.30×10^{-16}	1.48×10^{-16}
10 km	229.7	1.92×10^{-17}	5.32×10^{-20}	1.40×10^{-15}	1.51×10^{-16}
15 km	212.6	1.24×10^{-17}	3.94×10^{-20}	1.98×10^{-15}	1.56×10^{-16}
20 km	215.5	1.28×10^{-17}	4.15×10^{-20}	1.86×10^{-15}	1.55×10^{-16}
25 km	218.6	1.37×10^{-17}	4.38×10^{-20}	1.74×10^{-15}	1.54×10^{-16}
30 km	223.7	1.55×10^{-17}	4.79×10^{-20}	1.57×10^{-15}	1.53×10^{-16}

[a] k_R, k_{WM}, k_{WD}, and k_{SA} were respectively denoted the rate constants for the t-N_2O_4 + NH_3, t-N_2O_4 + NH_3···H_2O, t-N_2O_4 + NH_3···$(H_2O)_2$, and t-N_2O_4 + NH_3···H_2SO_4 reactions. [b] The 0–30 km data were reported from ref. 88 and 89.
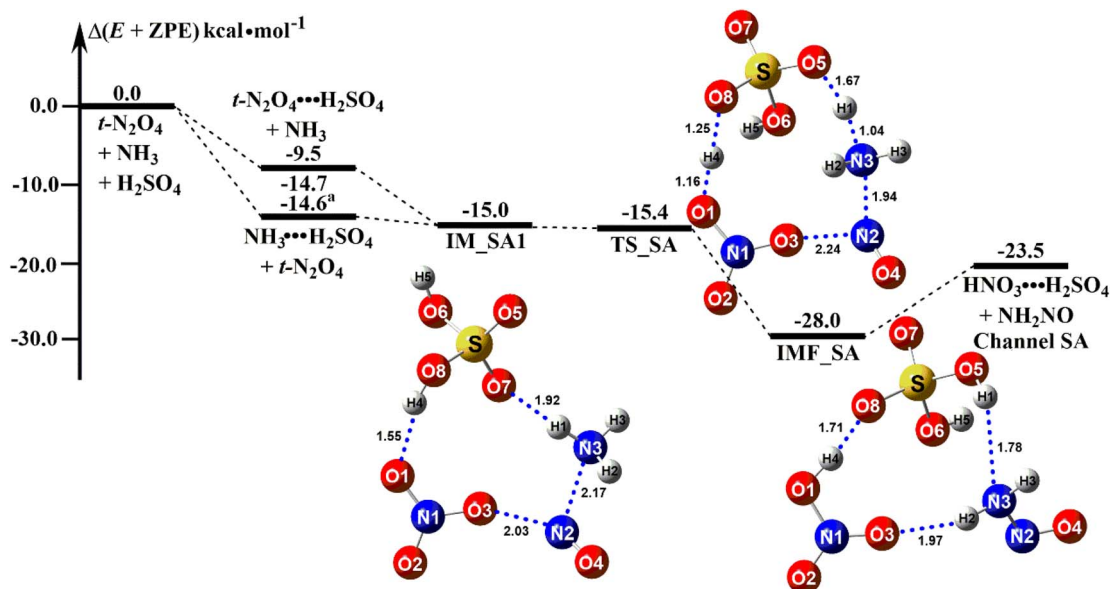
Fig. 3 Potential energy profiles for the t-N_2O_4 + NH_3 → HNO_3 + NH_2NO reaction catalyzed by H_2SO_4 at the CCSD(T)/aug-cc-pVTZ//B3LYP-D3/6-311++G(3df,2pd) level (a) The values was reported from ref. 92.

reactant complex IM_SA1. The rate constant of the t-N_2O_4 + $NH_3\cdots H_2SO_4$ reaction is one order of magnitude more than that of the ammonolysis reaction of t-N_2O_4 without a catalyst, as shown in Table 2. This result revealed that H_2SO_4 in the t-N_2O_4 + $NH_3\cdots H_2SO_4$ reaction plays a favorable catalytic role in promoting the ammonolysis reaction of t-N_2O_4. Thus, the ammonolysis reaction of t-N_2O_4 assisted by $(H_2O)_2$ and H_2SO_4 was more kinetically favorable than the reaction with H_2O.

3.4 Kinetics and implication in atmospheric chemistry

According to previous reports,[93–96] it is clear that the rate constant listed in Table 2 is insufficient to predict the atmospheric importance of the ammonolysis reaction of t-N_2O_4 assisted by $(H_2O)_2$ and H_2SO_4. To understand the atmospheric effect of $(H_2O)_2$ and H_2SO_4 on the ammonolysis reaction of t-N_2O_4, we introduced the effective rate constants (k') to calculate the relative efficiency of neutral and acid trace gases affecting the atmospheric reaction[97–100] and to compare the rate constant for the naked reaction.

On the basis of the rate constant for Channels WM, WD, and SA, the equilibrium constant for the bimolecular formation $(NH_3\cdots H_2O$, $NH_3\cdots(H_2O)_2$, and $NH_3\cdots H_2SO_4)$ and the concentrations of H_2O, $(H_2O)_2$, and H_2SO_4 are listed in Tables S4-6,† as stated in eqn (5)–(7).

$$k'_{WM} = k_{WM} \times K_{eq}(NH_3\cdots H_2O) \times [H_2O] \quad (5)$$

$$k'_{WD} = k_{WD} \times K_{eq}(NH_3\cdots(H_2O)_2) \times [(H_2O)_2] \quad (6)$$

$$k'_{SA} = k_{SA} \times K_{eq}(NH_3\cdots H_2SO_4) \times [H_2SO_4] \quad (7)$$

where k_{WM}, k_{WD}, and k_{SA} are the bimolecular rate constants for Channel WM, Channels WD, and SA, respectively; $K_{eq}(NH_3\cdots H_2O)$, $K_{eq}(NH_3\cdots(H_2O)_2)$, and $K_{eq}(NH_3\cdots H_2SO_4)$ are the equilibrium constants for the formation of complexes $NH_3\cdots H_2O$, $NH_3\cdots(H_2O)_2$, and $NH_3\cdots H_2SO_4$. $[H_2O]$, $[(H_2O)_2]$, and $[H_2SO_4]$ represent the concentrations of H_2O, $(H_2O)_2$, and H_2SO_4 taken from previous reports.[44,87] The k' for the ammonolysis reaction of t-N_2O_4 with X at 0 km altitude and at different altitudes (5–30 km) in the troposphere was calculated.

3.4.1 Zero kilometer altitude. As seen in Table 3, the calculated value of k'_{SA} can compete with k'_{WD} at 280 K. With increasing temperature, the calculated k'_{SA} was ~1–3 orders of magnitude smaller than the values of k'_{WD}, showing that the ammonolysis reaction of t-N_2O_4 was superior to that of an acidic

Table 3 The effective rate constants (k', cm^3 molecule^{-1} s^{-1}) for the t-N_2O_4 + NH_3 reaction assisted by H_2O, $(H_2O)_2$, and H_2SO_4 within the temperature range of 280–320 K^{a,b} (0 km)

Catalysts	T/K	280 K	290 K	298 K	300 K	310 K	320 K
k'_{WM}	100% RH^c	4.29×10^{-22}	6.96×10^{-22}	1.02×10^{-21}	1.11×10^{-21}	1.70×10^{-21}	2.49×10^{-21}
k'_{WD}	100% RH^c	2.45×10^{-21}	3.68×10^{-21}	5.16×10^{-21}	5.46×10^{-21}	7.70×10^{-21}	1.02×10^{-20}
k'_{SA}	$[H_2SO_4]^c = 10^8$ mol cm^3	1.39×10^{-21}	5.49×10^{-22}	2.72×10^{-22}	2.32×10^{-22}	1.03×10^{-22}	4.71×10^{-23}

^{a} k'_{WM}, k'_{WD}, and k'_{SA} were respectively denoted the effective rate constants for the t-N_2O_4 + $NH_3\cdots H_2O$, t-N_2O_4 + $NH_3\cdots(H_2O)_2$, and t-N_2O_4 + $NH_3\cdots H_2SO_4$ reactions. ^{b} The values of temperature were reported from ref. 88 and 89. ^{c} The values of concentrations were reported from ref. 44 and 87.

1412 | *Environ. Sci.: Atmos.*, 2023, **3**, 1407–1417

© 2023 The Author(s). Published by the Royal Society of Chemistry

Table 4 The effective rate constants (k', cm^3 molecule^{-1} s^{-1}) for the t-N$_2$O$_4$ + NH$_3$ reaction with H$_2$O, (H$_2$O)$_2$, and H$_2$SO$_4$ at different altitudes in troposphere[a]

Altitude (km)[b]	T (K)[b]	P (torr)[b]	k'_{WM}	k'_{WD}	k'_{SA}	k'_{SA}/k_{tot}
5	259.3	406.75	5.62×10^{-23}	1.50×10^{-22}	1.81×10^{-21}	5.05×10^{-5}
10	229.7	202.16	2.12×10^{-23}	1.74×10^{-22}	9.47×10^{-21}	4.93×10^{-4}
15	212.6	91.20	1.38×10^{-25}	2.95×10^{-26}	3.74×10^{-21}	3.02×10^{-4}
20	215.5	41.04	6.12×10^{-26}	4.52×10^{-27}	4.00×10^{-22}	3.11×10^{-5}
25	218.6	19.00	3.05×10^{-26}	8.56×10^{-28}	2.71×10^{-21}	1.97×10^{-4}
30	223.7	8.36	1.33×10^{-26}	1.12×10^{-28}	7.88×10^{-21}	5.06×10^{-4}

[a] k'_{WM}, k'_{WD}, and k'_{SA} were respectively denoted the effective rate constants for the t-N$_2$O$_4$ + NH$_3\cdots$H$_2$O, t-N$_2$O$_4$ + NH$_3\cdots$(H$_2$O)$_2$, and t-N$_2$O$_4$ + NH$_3\cdots$H$_2$SO$_4$ reactions; $k_{tot} = k_R + k'_{WD} + k'_{SA}$. [b] The values of altitude, temperature and pressure were reported from ref. 87, 88 and 89.

(H$_2$SO$_4$) catalyst in the presence of neutral (H$_2$O and (H$_2$O)$_2$) catalysts. However, the H$_2$SO$_4$-catalyzed reaction can be neglected because its calculated k'_{SA} was at least 4 orders of magnitude lower than the corresponding value of k_R in the naked reaction of the ammonolysis reaction of t-N$_2$O$_4$. This indicated that the contributions of H$_2$SO$_4$ to the ammonolysis reaction of t-N$_2$O$_4$ in atmospheric chemistry are not obvious within the temperature range of 280–320 K (at 0 km altitude).

3.4.2 Higher altitudes. The k' for the ammonolysis reaction of t-N$_2$O$_4$ with H$_2$O, (H$_2$O)$_2$, and H$_2$SO$_4$ were calculated within the 5–30 km altitude range, and the calculated k' is listed in Table 4. It can be seen in Table 4 that the contribution of H$_2$SO$_4$ was most obvious in the catalysts of H$_2$O, (H$_2$O)$_2$, and H$_2$SO$_4$ within the altitude range of 5–30 km, since the value of k'_{SA} was larger by 1–8 orders of magnitude than that of k'_{WD}. In order to quantitatively assess the impact of H$_2$SO$_4$ on the ammonolysis reaction of t-N$_2$O$_4$, the total rate constant k_{tot} can be calculated using eqn (8). The branching ratio for k'_{SA}/k_{tot} in Table 4 was calculated to be 3.11×10^{-5}–5.06×10^{-4} at 5–30 km. This indicates that the contribution of the H$_2$SO$_4$-assisted ammonolysis reaction of t-N$_2$O$_4$ can be negligible in atmospheric gas-phase chemistry.

$$k_{tot} = k_R + k'_{WD} + k'_{SA} \tag{8}$$

4. Summary and conclusions

In this work, the favorable route for the ammonolysis reaction of t-N$_2$O$_4$ in the presence of neutral (H$_2$O and (H$_2$O)$_2$) and acidic (H$_2$SO$_4$) catalysts was investigated using the quantum chemical method of CCSD(T)/aug-cc-pVTZ//B3LYP-D3/6-311++G(3df,2pd) and the master equation. The calculated results show that the energy barrier for the ammonolysis reaction of t-N$_2$O$_4$ increased when H$_2$O was present, but when (H$_2$O)$_2$ was present, the reaction energy barrier decreased to 0.3 kcal mol^{-1}, which was 3.4 kcal mol^{-1} lower than the ammonolysis reaction of t-N$_2$O$_4$ without the catalyst, especially when H$_2$SO$_4$ was directly involved in the reaction that is a barrierless process. In terms of the effective rate constant, (H$_2$O)$_2$ outperforms the other catalysts in the temperature range of 280–320 K (0 km). Moreover, the effect of H$_2$SO$_4$ on the ammonolysis reaction of t-N$_2$O$_4$ is obvious at higher altitudes of 5–30 km. Overall, this work will give a new insight into how the neutral and acidic catalysts affect the formation of HNO$_3$ from the ammonolysis reaction of t-N$_2$O$_4$. As HNO$_3$ is an important source of acid rain, the present work will provide a potential formation pathway for HNO$_3$, which plays a crucial role in the formation of acid rain.

Author contributions

Ruxue Mu: investigation, data curation, visualization, writing – original draft. Weixin Zhou: supervision, writing – review and editing, project administration. Zhaozhao Hong: visualization, data curation. Rui Wang: writing – review and editing, project administration. Quan Liu: visualization, data curation. Qiang Zhang: formal analysis. Min Jiang: formal analysis. Balaganesh Muthiah: supervision, writing – review and editing. Tianlei Zhang: writing – review and editing, project administration.

Conflicts of interest

The authors declare that they have no known competing financial interests or personal relationships that could have appeared to influence the work reported in this paper.

Acknowledgements

References

1 M. T. Martins-Costa, J. M. Anglada, J. S. Francisco and M. F. Ruiz-López, Theoretical investigation of the photoexcited NO$_2$ + H$_2$O reaction at the air-water interface and its atmospheric implications, *Chem. – Eur. J.*, 2019, **25**, 13899–13904.

2 A. Bacak, M. Cooke, M. Bardwell, M. McGillen, A. Archibald, L. Huey, D. Tanner, S. Utembe, M. Jenkin and R. Derwent, Kinetics of the HO$_2$ + NO$_2$ Reaction: On the impact of new

gas-phase kinetic data for the formation of HO_2NO_2 on HO_x, NO_x and HO_2NO_2 levels in the troposphere, *Atmos. Environ.*, 2011, **45**, 6414–6422.

3 J. H. Seinfeld and S. N. Pandis, *Atmospheric Chemistry and Physics: from Air Pollution to Climate Change*, John Wiley & Sons, 2016.

4 W.-G. Liu and W. A. Goddard III, First-principles study of the role of interconversion between NO_2, N_2O_4, *cis*-ONO-NO_2, and *trans*-ONO-NO_2 in chemical processes, *J. Am. Chem. Soc.*, 2012, **134**, 12970–12978.

5 C. Nonnenberg, I. Frank and T. M. Klapötke, Ultrafast cold reactions in the bipropellant monomethylhydrazine/ nitrogen tetroxide: CPMD simulations, *Angew. Chem., Int. Ed.*, 2004, **43**, 4586–4589.

6 L. Dejun, T. Gan, Y. Zhengwei, J. Guofeng, W. ZHANG, W. Yin and W. Huali, Stress corrosion behavior of 2195-T8 Al-Li alloy with an artificial pit exposed to a 30vol% HNO_3 solution, *Chin. J. Aeronaut.*, 2023, **36**, 304–315.

7 Y. Guo, Z. Huang, G. Tian, W. Wu, J. Lin and X. Chang, Isomerization and reaction process of $N_2O_4(H_2O)_n$, *RSC Adv.*, 2023, **13**, 12469–12475.

8 B. J. Finlayson-Pitts and J. N. Pitts Jr, *Chemistry of the Upper and Lower Atmosphere: Theory, Experiments, and Applications*, Elsevier, 1999.

9 T. Zhang, M. Wen, X. Cao, Y. Zhang, Z. Zeng, X. Guo, C. Zhao, M. Lily and R. Wang, The hydrolysis of NO_2 dimer in small clusters of sulfuric acid: A potential source of nitrous acid in troposphere, *Atmos. Environ.*, 2020, **243**, 117876.

10 L. Li, Z. Duan, H. Li, C. Zhu, G. Henkelman, J. S. Francisco and X. C. Zeng, Formation of HONO from the NH_3-promoted hydrolysis of NO_2 dimers in the atmosphere, *Proc. Natl. Acad. Sci.*, 2018, **115**, 7236–7241.

11 R. Zhu, K.-Y. Lai and M.-C. Lin, Ab initio chemical kinetics for the hydrolysis of N_2O_4 isomers in the gas phase, *J. Phys. Chem. A*, 2012, **116**, 4466–4472.

12 R. Putikam and M. C. Lin, A novel mechanism for the isomerization of N_2O_4 and its implication for the reaction with H_2O and acid rain formation, *Int. J. Quantum Chem.*, 2018, **118**, e25560.

13 H. P. Trac, T. Le Huyen and M.-C. Lin, A Computational Study on the Redox Reactions of Ammonia and Methylamine with Nitrogen Tetroxide, *J. Phys. Chem. A*, 2020, **124**, 9923–9932.

14 K. Mondal, S. Biswas, A. Chattopadhyay, P. Chatterjee and T. Chakraborty, Gas-phase oxidation of NO_2 to HNO_3 by phenol: atmospheric implications, *ACS Earth Space Chem.*, 2021, **5**, 2131–2141.

15 M. Wen, R. Li, T. Zhang, C. Ding, Y. Hu, R. Mu, M. Liang, T. Ou and B. Long, A potential source of tropospheric secondary organic aerosol precursors: The hydrolysis of N_2O_5 in water dimer and small clusters of sulfuric acid, *Atmos. Environ.*, 2022, **287**, 119245.

16 J. G. Calvert, A. Lazrus, G. L. Kok, B. G. Heikes, J. G. Walega, J. Lind and C. A. Cantrell, Chemical mechanisms of acid generation in the troposphere, *Nature*, 1985, **317**, 27–35.

17 J. I. Steinfeld, Atmospheric chemistry and physics: from air pollution to climate change, *Environ Sci Policy*, 1998, **40**, 26.

18 L. P. Viegas and A. n. J. Varandas, Role of $(H_2O)_n$ (n = 2-3) Clusters on the HO_2 + O_3 Reaction: A Theoretical Study, *J. Phys. Chem. B*, 2016, **120**, 1560–1568.

19 B. Long, J. L. Bao and D. G. Truhlar, Unimolecular reaction of acetone oxide and its reaction with water in the atmosphere, *Proc. Natl. Acad. Sci. U.S.A.*, 2018, **115**, 6135–6140.

20 X. Chen, C. Tao, L. Zhong, Y. Gao, W. Yao and S. Li, Theoretical study on the atmospheric reaction of SO_2 with the HO_2 and $HO_2\cdots H_2O$ complex formation HSO_4 and H_2SO_3, *Chem. Phys. Lett.*, 2014, **608**, 272–276.

21 R. J. Buszek, J. S. Francisco and J. M. Anglada, Water effects on atmospheric reactions, *Int. Rev. Phys. Chem.*, 2011, **30**, 335–369.

22 C. Iuga, J. R. Alvarez-Idaboy, L. Reyes and A. Vivier-Bunge, Can a single water molecule really catalyze the acetaldehyde + OH reaction in tropospheric conditions?, *J. Phys. Chem. Lett.*, 2010, **1**, 3112–3115.

23 B. Du and W. Zhang, Theoretical study on the water-assisted reaction of NCO with HCHO, *J. Phys. Chem. A*, 2013, **117**, 6883–6892.

24 P. S. Peters, D. Duflot, A. Faure, C. Kahane, C. Ceccarelli, L. Wiesenfeld and C. Toubin, Theoretical investigation of the isomerization of *trans*-HCOH to H_2CO: an example of a water-catalyzed reaction, *J. Phys. Chem. A*, 2011, **115**, 8983–8989.

25 B. Long, J. L. Bao and D. G. Truhlar, Atmospheric chemistry of Criegee intermediates: Unimolecular reactions and reactions with water, *J. Am. Chem. Soc.*, 2016, **138**, 14409–14422.

26 F. Xu, X.-F. Tan, Z.-G. Dong, D.-S. Ren and B. Long, Hydrolysis of ketene catalysed by nitric acid and water in the atmosphere, *Environ. Chem.*, 2020, **17**, 457–467.

27 K. Li, X. Song, T. Zhu, C. Wang, X. Sun, P. Ning and L. Tang, Mechanistic and kinetic study on the catalytic hydrolysis of COS in small clusters of sulfuric acid, *Environ. Pollut.*, 2018, **232**, 615–623.

28 B. Long, X.-F. Tan, C.-R. Chang, W.-X. Zhao, Z.-W. Long, D.-S. Ren and W.-J. Zhang, Theoretical studies on gas-phase reactions of sulfuric acid catalyzed hydrolysis of formaldehyde and formaldehyde with sulfuric acid and $H_2SO_4\cdots H_2O$ complex, *J. Phys. Chem. A*, 2013, **117**, 5106–5116.

29 X.-F. Tan, B. Long, D.-S. Ren, W.-J. Zhang, Z.-W. Long and E. Mitchell, Atmospheric chemistry of CH_3CHO: the hydrolysis of CH_3CHO catalyzed by H_2SO_4, *Phys. Chem. Chem. Phys.*, 2018, **20**, 7701–7709.

30 R. J. Buszek, A. Sinha and J. S. Francisco, The isomerization of methoxy radical: intramolecular hydrogen atom transfer mediated through acid catalysis, *J. Am. Chem. Soc.*, 2011, **133**, 2013–2015.

31 J. Elm, M. Bilde and K. V. Mikkelsen, Influence of nucleation precursors on the reaction kinetics of methanol with the OH radical, *J. Phys. Chem. A*, 2013, **117**, 6695–6701.

1414 | *Environ. Sci.: Atmos.*, 2023, **3**, 1407–1417

© 2023 The Author(s). Published by the Royal Society of Chemistry

32 A. Karton, Inorganic acid-catalyzed tautomerization of vinyl alcohol to acetaldehyde, *Chem. Phys. Lett.*, 2014, **592**, 330–333.

33 M. Torrent-Sucarrat, J. S. Francisco and J. M. Anglada, Sulfuric acid as autocatalyst in the formation of sulfuric acid, *J. Am. Chem. Soc.*, 2012, **134**, 20632–20644.

34 Y. Zhang, Y. Cheng, T. Zhang, R. Wang, J. Ji, Y. Xia, M. Lily, Z. Wang and B. Muthiah, A computational study of the $HO_2 + SO_3 \rightarrow HOSO_2 + {}^3O_2$ reaction catalyzed by a water monomer, a water dimer and small clusters of sulfuric acid: kinetics and atmospheric implications, *Phys. Chem. Chem. Phys.*, 2022, **24**, 18205–18216.

35 T. Zhang, Y. Zhang, S. Tian, M. Zhou, D. Liu, L. Lin, Q. Zhang, R. Wang and B. Muthiah, Possible atmospheric source of NH_2SO_3H: the hydrolysis of $HNSO_2$ in the presence of neutral, basic, and acidic catalysts, *Phys. Chem. Chem. Phys.*, 2022, **24**, 4966–4977.

36 Y. Cheng, R. Wang, Y. Chen, S. Tian, N. Gao, Z. Zhang and T. Zhang, Hydrolysis of SO_3 in Small Clusters of Sulfuric Acid: Mechanistic and Kinetic Study, *ACS Earth Space Chem.*, 2022, **6**, 3078–3089.

37 J. Liu, S. Fang, Z. Wang, W. Yi, F.-M. Tao and J.-y. Liu, Hydrolysis of sulfur dioxide in small clusters of sulfuric acid: Mechanistic and kinetic study, *Environ. Sci. Technol.*, 2015, **49**, 13112–13120.

38 T. Zhang, R. Wang, H. Chen, S. Min, Z. Wang, C. Zhao, Q. Xu, L. Jin, W. Wang and Z. Wang, Can a single water molecule really affect the $HO_2 + NO_2$ hydrogen abstraction reaction under tropospheric conditions?, *Phys. Chem. Chem. Phys.*, 2015, **17**, 15046–15055.

39 S. Sarkar and B. Bandyopadhyay, Aldehyde as a potential source of aminol in troposphere: Influence of water and formic acid catalysis on ammonolysis of formaldehyde, *Atmos. Environ.*, 2019, **213**, 223–230.

40 Z. Wang, C. Zhang, G. Lv, X. Sun, N. Wang and Z. Li, Synergistic reaction of SO_2 with NO_2 in presence of H_2O and NH_3: A potential source of sulfate aerosol, *Int. J. Mol. Sci.*, 2019, **20**, 3746.

41 B. Du and W. Zhang, The effect of $(H_2O)_n$ ($n = 1$–2) or H_2S on the hydrogen abstraction reaction of H_2S by OH radicals in the atmosphere, *Comput. Theor. Chem.*, 2015, **1069**, 77–85.

42 T. Zhang, W. Wang, P. Zhang, J. Lü and Y. Zhang, Water-catalyzed gas-phase hydrogen abstraction reactions of CH_3O_2 and HO_2 with HO_2: a computational investigation, *Phys. Chem. Chem. Phys.*, 2011, **13**, 20794–20805.

43 M. E. Dunn, E. K. Pokon and G. C. Shields, Thermodynamics of forming water clusters at various temperatures and pressures by Gaussian-2, Gaussian-3, complete basis set-QB3, and complete basis set-APNO model chemistries; implications for atmospheric chemistry, *J. Am. Chem. Soc.*, 2004, **126**, 2647–2653.

44 H. Zhang, O. Kupiainen-Määttä, X. Zhang, V. Molinero, Y. Zhang and Z. Li, The enhancement mechanism of glycolic acid on the formation of atmospheric sulfuric acid-ammonia molecular clusters, *J. Chem. Phys.*, 2017, **146**, 184308.

45 L. Zhang and B. Long, Hydrolysis of formyl fluoride catalyzed by sulfuric acid and formic acid in the atmosphere, *ACS Omega*, 2019, **4**, 18996–19004.

46 R. Asatryan and E. Ruckenstein, Dihydrogen catalysis: a remarkable avenue in the reactivity of molecular hydrogen, *Catal. Rev.*, 2014, **56**, 403–475.

47 S. Grimme, S. Ehrlich and L. Goerigk, Effect of the damping function in dispersion corrected density functional theory, *J. Comput. Chem.*, 2011, **32**, 1456–1465.

48 J. Witte, M. Goldey, J. B. Neaton and M. Head-Gordon, Beyond energies: Geometries of nonbonded molecular complexes as metrics for assessing electronic structure approaches, *J. Chem. Theory Comput.*, 2015, **11**, 1481–1492.

49 J. Rezac, Non-covalent interactions atlas benchmark data sets 2: Hydrogen bonding in an extended chemical space, *J. Chem. Theory Comput.*, 2020, **16**, 6305–6316.

50 J. Řezáč, An integrative framework for computational chemistry, *J. Comput. Chem.*, 2016, **37**, 1230–1237.

51 J. Elm, M. Bilde and K. V. Mikkelsen, Assessment of density functional theory in predicting structures and free energies of reaction of atmospheric prenucleation clusters, *J. Chem. Theory Comput.*, 2012, **8**, 2071–2077.

52 N. Mardirossian and M. Head-Gordon, How accurate are the Minnesota density functionals for noncovalent interactions, isomerization energies, thermochemistry, and barrier heights involving molecules composed of main-group elements?, *J. Chem. Theory Comput.*, 2016, **12**, 4303–4325.

53 A. T. Pereira, A. J. Ribeiro, P. A. Fernandes and M. J. Ramos, Benchmarking of density functionals for the kinetics and thermodynamics of the hydrolysis of glycosidic bonds catalyzed by glycosidases, *Int. J. Quantum Chem.*, 2017, **117**, e25409.

54 M. J. Frisch, G. W. Trucks, H. B. Schlegel, G. E. Scuseria, M. A. Robb, J. R. Cheeseman, G. Scalmani, V. Barone, B. Mennucci, G. A. Petersson and *et al.*, *Gaussian09*, 1, Gaussian, Inc., Wallingford CT, 2009, 121, pp. 150–166.

55 J. Elm, M. Bilde and K. V. Mikkelsen, Assessment of binding energies of atmospherically relevant clusters, *Phys. Chem. Chem. Phys.*, 2013, **15**, 16442–16445.

56 A. F. Rodrigues-Oliveira, F. W. M. Ribeiro, G. Cervi and T. C. Correra, Evaluation of common theoretical methods for predicting infrared multiphotonic dissociation vibrational spectra of intramolecular hydrogen-bonded ions, *ACS Omega*, 2018, **3**, 9075–9085.

57 M. Kieninger and O. N. Ventura, Calculations of the infrared and Raman spectra of simple thiols and thiol-water complexes, *Int. J. Quantum Inf.*, 2011, **111**, 1843–1857.

58 H. Hratchian and H. Schlegel, Using Hessian updating to increase the efficiency of a Hessian based predictor-corrector reaction path following method, *J. Chem. Theory Comput.*, 2005, **1**, 61–69.

59 H. P. Hratchian and H. B. Schlegel, Accurate reaction paths using a Hessian based predictor-corrector integrator, *J. Chem. Phys.*, 2004, **120**, 9918–9924.

60 S. Maeda, Y. Harabuchi, Y. Ono, T. Taketsugu and K. Morokuma, Intrinsic reaction coordinate: Calculation,

© 2023 The Author(s). Published by the Royal Society of Chemistry

Environ. Sci.: Atmos., 2023, **3**, 1407–1417 | 1415

bifurcation, and automated search, *Int. J. Quantum Chem.*, 2015, **115**, 258–269.

61 J. Pople, R. Krishnan, H. Schlegel and J. Binkley, Electron correlation theories and their application to the study of simple reaction potential surfaces, *Int. J. Quantum Chem.*, 1978, **14**, 545–560.

62 Y. S. Lee, S. A. Kucharski and R. J. Bartlett, A coupled cluster approach with triple excitations, *J. Chem. Phys.*, 1984, **81**, 5906–5912.

63 R. A. Kendall, T. H. Dunning Jr and R. J. Harrison, Electron affinities of the first-row atoms revisited. Systematic basis sets and wave functions, *J. Chem. Phys.*, 1992, **96**, 6796–6806.

64 T. J. Lee and P. R. Taylor, A diagnostic for determining the quality of single-reference electron correlation methods, *Int. J. Quantum Chem.*, 1989, **36**, 199–207.

65 T. J. Lee, Comparison of the T_1 and D_1 diagnostics for electronic structure theory: a new definition for the open-shell D_1 diagnostic, *Chem. Phys. Lett.*, 2003, **372**, 362–367.

66 J. Zhang and M. Dolg, ABCluster: the artificial bee colony algorithm for cluster global optimization, *Phys. Chem. Chem. Phys.*, 2015, **17**, 24173–24181.

67 J. Zhang and M. Dolg, Global optimization of clusters of rigid molecules using the artificial bee colony algorithm, *Phys. Chem. Chem. Phys.*, 2016, **18**, 3003–3010.

68 W. L. Jorgensen, J. Chandrasekhar, J. D. Madura, R. W. Impey and M. L. Klein, Comparison of simple potential functions for simulating liquid water, *J. Chem. Phys.*, 1983, **79**, 926–935.

69 D. J. Wales and M. P. Hodges, Global minima of water clusters $(H_2O)_n$, $n \leq 21$, described by an empirical potential, *Chem. Phys. Lett.*, 1998, **286**, 65–72.

70 A. D. MacKerell Jr, D. Bashford, M. Bellott, R. L. Dunbrack Jr, J. D. Evanseck, M. J. Field, S. Fischer, J. Gao, H. Guo and S. Ha, All-atom empirical potential for molecular modeling and dynamics studies of proteins, *J. Phys. Chem. B*, 1998, **102**, 3586–3616.

71 J. J. Stewart, Optimization of parameters for semiempirical methods VI: more modifications to the NDDO approximations and re-optimization of parameters, *J. Mol. Model.*, 2013, **19**, 1–32.

72 J. Stewart, *MOPAC2016 Stewart Computational Chemistry*, Colorado Springs, CO, OpenMOPAC, 2016.

73 Y. Chuang, J. Corchado, P. Fast, J. Villa, E. Coitino, W. Hu, Y. Liu, G. Lynch, K. Nguyen and C. Jackels, *Polyrate-version 8.2*, University of Minnesota, Minneapolis, 1999.

74 D. R. Glowacki, C.-H. Liang, C. Morley, M. J. Pilling and S. H. Robertson, MESMER: an open-source master equation solver for multi-energy well reactions, *J. Phys. Chem. A*, 2012, **116**, 9545–9560.

75 G. Horváth, I. Horváth, S. A.-D. Almousa and M. Telek, Numerical inverse Laplace transformation using concentrated matrix exponential distributions, *Perform. Evaluation*, 2020, **137**, 102067.

76 A. Kumar, S. Mallick and P. Kumar, Oxidation of HOSO˙ by Cl˙: a new source of SO_2 in the atmosphere?, *Phys. Chem. Chem. Phys.*, 2021, **23**, 18707–18711.

77 T. V.-T. Mai, M. V. Duong, H. T. Nguyen and L. K. Huynh, Ab initio kinetics of the $HOSO_2$ + $^3O_2$ → SO_3 + HO_2 reaction, *Phys. Chem. Chem. Phys.*, 2018, **20**, 6677–6687.

78 S. Mallick, A. Kumar and P. Kumar, Oxidation of HOSO by NH_2: A new path for the formation of an acid rain precursor, *Chem. Phys. Lett.*, 2021, **773**, 138536.

79 H. Hippler, J. Troe and H. Wendelken, Collisional deactivation of vibrationally highly excited polyatomic molecules. II. Direct observations for excited toluene, *J. Chem. Phys.*, 1983, **78**, 6709–6717.

80 R. J. Kee, G. Dixon-Lewis, J. Warnatz, M. E. Coltrin and J. A. Miller, A Fortran computer code package for the evaluation of gas-phase multicomponent transport properties, *Sandia National Laboratories Report SAND86-8246*, 1986, vol. 13, pp. 80401–81887.

81 T. V.-T. Mai, H. T. Nguyen and L. K. Huynh, Ab initio dynamics of hydrogen abstraction from N_2H_4 by OH radicals: an RRKM-based master equation study, *Phys. Chem. Chem. Phys.*, 2019, **21**, 23733–23741.

82 T. V.-T. Mai, H. T. Nguyen and L. K. Huynh, Kinetics of hydrogen abstraction from CH_3SH by OH radicals: An *ab initio* RRKM-based master equation study, *Atmos. Environ.*, 2020, **242**, 117833.

83 X. T. Le, T. V.-T. Mai, M. v. Duong and L. K. Huynh, Kinetics of hydrogen abstraction from desflurane by OH and Cl radicals–A theoretical study, *Chem. Phys. Lett.*, 2019, **728**, 142–147.

84 T. V.-T. Mai, P. Raghunath, X. T. Le, L. K. Huynh, P.-C. Nam and M.-C. Lin, Ab initio chemical kinetics for the HCCO + OH reaction, *Chem. Phys. Lett.*, 2014, **592**, 175–181.

85 T. V.-T. Mai, M. v. Duong, H. T. Nguyen, K. C. Lin and L. K. Huynh, Ab initio chemical kinetics of the CH_2OO + C_2F_4 reaction, *Chem. Phys. Lett.*, 2018, **706**, 280–284.

86 T. V.-T. Mai and L. K. Huynh, Ab initio kinetics of the C_2H_2 + NH_2 reaction: a revisited study, *Phys. Chem. Chem. Phys.*, 2019, **21**, 17232–17239.

87 J. M. Anglada, G. J. Hoffman, L. V. Slipchenko, M. M. Costa, M. F. Ruiz-Lopez and J. S. Francisco, Atmospheric significance of water clusters and ozone-water complexes, *J. Phys. Chem. A*, 2013, **117**, 10381–10396.

88 B. Bandyopadhyay, P. Kumar and P. Biswas, Ammonia catalyzed formation of sulfuric acid in troposphere: the curious case of a base promoting acid rain, *J. Phys. Chem. A*, 2017, **121**, 3101–3108.

89 S. Mallick, S. Sarkar, B. Bandyopadhyay and P. Kumar, Effect of ammonia and formic acid on the OH˙ + HCl reaction in the troposphere: Competition between single and double hydrogen atom transfer pathways, *J. Phys. Chem. A*, 2018, **122**, 350–363.

90 T. Zhang, K. Zhai, Y. Zhang, L. Geng, Z. Geng, M. Zhou, Y. Lu, X. Shao and M. Lily, Effect of water and ammonia on the HO + NH_3 → NH_2 + H_2O reaction in troposphere: Competition between single and double hydrogen atom transfer pathways, *Comput. Theor. Chem.*, 2020, **1176**, 112747.

91 S. Sarkar and B. Bandyopadhyay, Theoretical investigation of the relative impacts of water and ammonia on the

1416 | *Environ. Sci.: Atmos.*, 2023, **3**, 1407–1417

© 2023 The Author(s). Published by the Royal Society of Chemistry

tropospheric conversion of N$_2$O$_5$ to HNO$_3$, *Phys. Chem. Chem. Phys.*, 2021, **23**, 6651–6664.

92 B. Long, X. F. Tan, Y. B. Wang, J. Li, D. S. Ren and W. J. Zhang, Theoretical Studies on Reactions of OH with H$_2$SO$_4$···NH$_3$ Complex and NH$_2$ with H$_2$SO$_4$ in the Presence of Water, *ChemistrySelect*, 2016, **1**, 1421–1430.

93 S. Sarkar, S. Mallick, P. Kumar and B. Bandyopadhyay, Isomerization of methoxy radical in the troposphere: competition between acidic, neutral and basic catalysts, *Phys. Chem. Chem. Phys.*, 2017, **19**, 27848–27858.

94 R. J. Buszek, M. Torrent-Sucarrat, J. M. Anglada and J. S. Francisco, Effects of a single water molecule on the OH + H$_2$O$_2$ reaction, *J. Phys. Chem. A*, 2012, **116**, 5821–5829.

95 J. Gonzalez, J. M. Anglada, R. J. Buszek and J. S. Francisco, Impact of water on the OH + HOCl reaction, *J. Am. Chem. Soc.*, 2011, **133**, 3345–3353.

96 A. Parandaman, J. E. Perez and A. Sinha, Atmospheric decomposition of trifluoromethanol catalyzed by formic acid, *J. Phys. Chem. A*, 2018, **122**, 9553–9562.

97 G. Shen, M. Suto and L. Lee, Reaction rate constant of SO$_3$ + CH$_3$OH in the gas phase, *Int. J. Chem. Kinet.*, 1990, **22**, 633–639.

98 L. Liu, J. Zhong, H. Vehkamäki, T. Kurtén, L. Du, X. Zhang, J. S. Francisco and X. C. Zeng, Unexpected quenching effect on new particle formation from the atmospheric reaction of methanol with SO$_3$, *Proc. Natl. Acad. Sci.*, 2019, **116**, 24966–24971.

99 J. Gonzalez, M. Torrent-Sucarrat and J. M. Anglada, The reactions of SO$_3$ with HO$_2$ radical and H$_2$O···HO$_2$ radical complex. Theoretical study on the atmospheric formation of HSO$_5$ and H$_2$SO$_4$, *Phys. Chem. Chem. Phys.*, 2010, **12**, 2116–2125.

100 Y.-Q. Sun, X. Wang, F.-Y. Bai and X.-M. Pan, Theoretical study of the hydrolysis of HOSO + NO$_2$ as a source of atmospheric HONO: effects of H$_2$O or NH$_3$, *Environ. Chem.*, 2016, **14**, 19–30.

© 2023 The Author(s). Published by the Royal Society of Chemistry

Environ. Sci.: Atmos., 2023, **3**, 1407–1417 | **1417**